# Rapid Ultra-Sensitive Single Particle Surface Enhanced Raman Spectroscopy using Metallic Nanopores

*Michael P. Cecchini,*[†,§] *Aeneas Wiener,*[‡,§] *Vladimir A. Turek,*[†] *Hyangh Chon,*[‖] *Sangyeop Lee,*[‖] *Aleksandar P. Ivanov,*[†] *David W. McComb,*[⊥] *Jaebum Choo,*[‖] *Tim Albrecht,*[†] *Stefan A. Maier,*[‡] *Joshua B. Edel*[†*]

[†]Department of Chemistry, Imperial College London, South Kensington Campus, London, SW7 2AZ.
‡Department of Physics, Imperial College London, South Kensington Campus, London, SW7 2AZ.
[‖]Department of Bionano Engineering, Hanyang University, Ansan 426-791, South Korea.
[⊥]Department of Materials Science and Engineering, The Ohio State University, Columbus, OH. 43210.

Corresponding author: joshua.edel@imperial.ac.uk

[§] These authors contributed equally to this work

Keywords: Raman spectroscopy, surface enhanced Raman spectroscopy, nanoparticles, nanopore, plasmonics, nanoplasmonics, metallic nanopore, optical sensor, single molecule sensors.

**Abstract**

Nanopore sensors embedded within thin dielectric membranes have been gaining significant interest due to their single molecule sensitivity and compatibility of detecting a large range of analytes, from DNA and proteins, to small molecules and particles. Building on this concept we utilize a metallic Au solid-state membrane to translocate and rapidly detect single Au nanoparticles (NPs) functionalized with 589 dye molecules using surface enhanced resonance Raman Spectroscopy (SERRS). We show that due to the plasmonic coupling between the Au metallic nanopore surface and the NP, signal intensities are enhanced when probing analyte molecules bound to the NP surface. Although not single molecule, this nanopore sensing scheme benefits from the ability of SERS to provide rich vibrational information on the analyte, improving on current nanopore-based electrical and optical detection techniques. We show that the full vibrational band of the analyte can be detected with ultra-high spectral sensitivity, and rapid temporal resolution of 880 μs.

Nanopore sensing has recently become a highly regarded technique for applications where single analyte analysis is required[1, 2, 3, 4]. A number of nanopore platforms exist, *e.g.* the cell membrane where they are used for ion transport. They can also be synthetically produced using either biological building blocks and/or solid-state semiconductor processing materials[5]. The general underlying theme is that the nanopore is embedded in an ultra-thin membrane with a similar thickness to that of the lateral dimensions of the nanopore. Although all methods have their pros and cons, membrane stability, limited size range, nanopore stability, material selection, and fragility are often touted as potential stumbling blocks when using a biological nanopore for sensing applications[1]. Although not all these limitations can necessarily be circumvented when using solid-state nanopores, significant advantages are worth highlighting. Firstly, the membrane can be made from any material that can be deposited or fabricated using conventional semiconductor processing techniques. For example, low stress silicon nitride ($SiN_x$) tends to be a material of choice amongst most users, although other materials such as $SiO_2$[6], SiC[7], $Al_2O_3$[2], graphene[8] and even metals such as Al[9, 10, 11], Au[12], and Pt[13] have been used for specific applications. Secondly the nanopore (or even ordered arrays of nanopores) embedded within the membrane can be precisely sculpted with sizes ranging from 1 nm upwards which allows for precise tuning of the nanopore size to the dimensions of the analyte.

To date, nanopore sensors have been used to detect a large variety of analytes at the single molecule level. For example, nucleic acid and protein analysis has perhaps been the most popular[1, 14, 15]. The predominant method used for the detection of a translocation event (i.e. passing of analytes through the nanopore) relies on electrical means using what is typically termed ionic current blockade sensing[5] (ESI Figure 1). Aside from electrical detection, optical fluorescence detection has also been used to successfully monitor translocation events using membranes made from $SiN_x$ or a combination of $SiN_x$ and aluminum[9, 16, 17]. The inherent advantages in doing so are both the possibility of probing multiple pores simultaneously and not being restricted to high electrolyte concentrations to increase the current change. Furthermore, fluorescent labels can be used to probe localized subsets of the analyte as opposed to the entire molecule. There have also been examples of combining both electrical and optical detection to maximize the information that can be extracted from each and every single molecule translocating through the nanopore[17].

Building on using optical fluorescence techniques as a detection mechanism, this can also be extended to label-free vibrational methods, e.g. Raman spectroscopy. If sufficiently sensitive, this approach would allow for “molecular fingerprinting” which would supply unique information complimentary to electrical and fluorescence detection. Unfortunately, Raman spectroscopy typically requires high analyte

concentrations and long measurement times due to the low scattering cross-section making this technique impractical for nanopore sensing where sub 10 ms translocation times are the norm. Alternatively, surface enhanced Raman spectroscopy (SERS) results in higher scattering cross sections decreasing the acquisition times required, and in some cases makes single particle and molecule detection possible[18, 19, 20, 21]. Sensitivity can be increased further by matching the excitation frequency with the electronic transition of the analyte, a condition known as resonance Raman (RR) or SERRS. Multiple forms of SER(R)S active substrates exist[22, 23, 24, 25]; however, both single and aggregated metallic nanoparticles (NPs) continue to be the most popular due to their ease of fabrication and ability to act as mobile SERS substrates[26, 27, 28]. As will be shown nanopores can be used to facilitate the rapid detection of single NPs while still collecting full vibrationally rich spectral information of the analyte. Importantly, NP translocation events, of both metallic and non-metallic particles, using $SiN_x$ solid-state nanopores have already been documented albeit by characterizing the translocation events using electrical means using a high ionic strength solution[29, 30, 31]. Generally speaking such a high ionic strength would typically aggregate larger unprotected Au NPs. In this article we detect Au NPs functionalized with malachite green isothiocyanate (MGITC) electrophoretically driven through an $Au/SiN_x$ solid-state membrane using SERRS. By doing so, we show that not only can SERRS be used to efficiently and rapidly detect (< 1 ms time resolution) single metallic Au NPs within a nanopore (Figure 1a), but, perhaps more importantly, due to plasmonic coupling between the Au metallic nanopore surface and the NP, signal intensities are significantly enhanced when probing analyte molecules bound to the NP.

To realize and characterize this platform, devices were fabricated using a combination of wet and reactive ion etching (RIE) and thin film deposition[13, 32]. Each Si chip has a 5 x 5 mm footprint (300 μm thick) consisting of a 50 nm layer of low stress $SiN_x$, a 5 nm Ti adhesion layer, and 100 nm thick Au layer. Precise details of the fabrication process can be found in the supporting information (ESI Figure 2). A free standing $SiN_x$/Au 94 μm x 94 μm membrane was fabricated by removing a patterned area of the Si using KOH wet etching, Figure 1b. Nanopores with a diameter of 80 +/- 10 nm were milled into the $SiN_x$/Au membrane with a $Ga^+$ focused ion beam using a 5 pA beam current for a duration of 3 s (Figure 1c). Alignment marks consisting of two circular rings were also partially milled into the $SiN_x$ membrane to act as a visual aid to easily locate the nanopore. The complete device was then packaged into a fluidic cell separating the solution filled compartments, each incorporating a non-polarizable Ag/AgCl electrode. The Turkevich-Frens method[33, 34] was used to synthesize Au NPs that were measured to be 53.3 ± 18.0 nm using dynamic light scattering (DLS). These NPs were labeled with MGITC ( ≈ 589 MGITC molecules/particle[23]) and stabilized with poly(acrylic acid) ($M_w$ ≈ 1800). Exact NP synthesis parameters are described in the ESI Figure 3. SEM and DLS characterization of the NPS are shown in the ESI Figure

4. The final NP hydrodynamic diameter after synthesis was measured to be 57.1 ± 24.4 nm. UV-Vis of the NPs before and after functionalization with MGITC showed no signs of aggregation (see ESI Figure 3). DLS also confirmed that no aggregation occurred (ESI Figure 4b, c). It should be stressed that DLS measures the hydrodynamic radius of the colloid rather than the actual size of the metallic core[35]. Since the plasmonic enhancement will be governed by the core metallic NP size not the hydrodynamic diameter, the simulations were performed using a 40 nm core diameter, which matches more closely to the physical size of the NPs used. It should also be noted that the absorbance maximum for MGITC overlaps with the excitation wavelength used for acquiring the spectra hence SERRS and not SERS is being measured[36] (ESI Figure 5). To date, previous approaches of detecting single NPs have relied on resonance with the analyte creating an additional enhancement[26, 28], and/or have relied on unique NP shapes[27].

Translocation experiments were carried out on a custom built Raman microscope[22, 26] using a HeNe 632.8 nm excitation source focused to a diffraction limited spot at the Au nanopore entrance with the particles loaded in the bottom chamber (ESI Figure 6). This arrangement proved successful; however, ultra-low concentrations of NPs (≈ 2.5 pM dispersed in 1 mM NaCl) were required to minimize the potential of unwanted detection events not coming from NP translocations. It should be noted that the signal coming from NPs diffusing in and around the vicinity of the detection volume was negligible compared to the field-enhanced signal coming from coupling of the nanopore wall to the NP during a translocation event. As such, the NPs in the lower reservoir remained nearly invisible.

We characterize our system using a fully retarded, three-dimensional, electrodynamic finite element model of the field enhancement experienced by a NP moving through a metallic nanopore. Figure 1d shows the strong electromagnetic field enhancement that occurs at the contact point between the NP and the nanopore wall. In contrast to this, Figure 1e shows that a single Au NP, located in water, experiences only a moderate $|E_{max}/E_0|$ field enhancement of 4 at its dipolar resonance of 550 nm (dotted line). However, as the NP reaches the center of the pore (dashed line in Figure 1e), the field enhancement increases to 10. This increased field enhancement is concomitant with a broadening and red-shifting of the dipolar resonance to 600 nm due to the hybridization of the plasmonic modes in the coupled NP-hole geometry. This is also highly beneficial when considering a 632.8 nm excitation source is used maximizing the enhancement. As the nanoparticle moves closer to the wall (solid line in Figure 1e) the mode red-shifts further and a quadrupolar mode emerges (see ESI Figure 7 for identification of modes). The broadband field enhancement achieved by this hybridized plasmonic system is highly beneficial for SERS as it allows for the simultaneous detection of resonance bands at different energies. Figure 1d

shows that the highest field enhancement caused by a NP moving along a vertical path through the nanopore always occurs at the entrance to the pore, where it reaches a value of 10 for a path through the center of the pore (red line), increasing to 20 and 60 for paths with reduced particle-wall distances of 5 nm and 3 nm respectively (green and blue lines).

Comparisons between the experimentally derived EF and the simulated EF were performed by comparing the simulated electric field enhancement from the nanopore on the NP to that of a single isolated metallic NP (taken from Figure 1e). Depending on the NP position within the nanopore, a maximum EF of 32 (x, z = 0) and $1.5x10^5$ (x, z = 17, 0 nm) was calculated for the 1174 $cm^{-1}$ vibrational band (683.6 nm). The average enhancement over the entire NP surface for the wavelength corresponding to the 1174 $cm^{-1}$ vibrational band (ESI Figure 7b) is slightly lower, EF = 27 and 132, for the two NP positions, respectively. Importantly, the enhancement is strongly dependant on the excitation wavelength which can be tuned to maximize overall enhancement to achieve maximum sensitivity, (ESI Figure 7a, b). Likewise, when considering the experimental system used in this study (i.e. 632.8 nm excitation and Stokes scattering measurements) the wavelength corresponding to the vibrational band of interest is also important, as the e-field enhancement varies significantly between 632.8-800 nm. For example, the 1174 $cm^{-1}$ vibrational band experiences an average EF of 27 and 132 while the 1364 $cm^{-1}$ vibrational band (692.6 nm) experiences an average EF of 25 and 247 for the different NP positions. Monitoring the 1616 $cm^{-1}$ vibrational band (704.9 nm) the average EF changes to 22 and 429. This clearly shows a strong enhancement dependence on the wavelength of the vibrational band which is further shown in ESI Figure 8 by overlaying the vibrational spectrum of MGITC with the simulated maximum electric field enhancement.

An example of a typical NP translocation event is shown in Figure 2a using a bias voltage of 750 mV. The spectra were background subtracted using an asymmetric least squares smoothing function which allowed direct intensity comparisons between a translocation and non-translocating nanoparticle detection event. The rapid CCD frame rate used for all acquisitions was 1136 Hz resulting in spectral information being recorded with an 880 μs time resolution. In this example, the translocation duration lasts 24.6 ms. The average translocation time for a 750 mV applied bias was measured to be 57.56 ± 29.8 ms. Histograms showing the spread in the translocation times for 500 and 750 mV applied biases are included in the ESI Figure 9. This translocation time is an order of magnitude longer than other nanoparticle translocation times previously reported using electrical detection methods[29, 31]. Unlike in previous reports where the nanopore surface was modified to change the surface charge groups[29], the $SiN_x$ pore remains negatively charged. As a result, a lengthened translocation time due to electroosmotic drag within the

nanopore is expected. Cyclic voltammetry[37, 38, 39].was used to gauge whether an interaction between the NPs and a gold surface exists which could lead to longer translocation times. The decrease in capacitance of the gold electrode over time indicated that an interaction between the two existed which could contribute to the long apparent translocation times (ESI Figure 10). Additional optical trapping of the NPs within the nanopore is unlikely at the excitation frequency used in our experiments, which is close to the LSPR energy of the NP. At optical energies near the LSPR the optical gradient force (responsible for trapping) is small compared to both scattering and absorption forces[40]. Importantly, the electrophoretic force on the nanoparticles in our experiments is much higher than previously reported optical trapping forces.

To compare the difference in SERRS intensity, Figure 2b shows a NP event diffusing through the detection volume in bulk solution without the presence of a nanopore. On average an increase of 320% is observed for the 1174 $cm^{-1}$ vibrational band due to the confinement and enhancement of the SERRS signal with the nanopore walls. Furthermore the signal to noise ratio is also increased on average by 79%. The wavelength corresponding to the 1174 $cm^{-1}$ vibrational band is 683.6 nm and as can be seen from Figure 1e shows significant enhancement when the NP is near the nanopore. Importantly, vibrational bands red-shifted from the 1174 $cm^{-1}$ are expected to undergo even further enhancement. For example the intensity of the 1364 and 1616 $cm^{-1}$ vibrational bands increase from 293 to 1948 photons and 217 to 1781 photons, respectively. This results in a 567 and 720% signal increase.

Examples of isolating two modes of vibrations for MGITC (1174 $cm^{-1}$ and 1364 $cm^{-1}$) are shown as time dependent traces using a time resolution of 880 μs, Figure 3a, rebinned to 8.8 ms. The average signal intensity of the 1174 $cm^{-1}$ vibrational band over the entire time trace was measured to be 3884 ± 1394 photons and translocation times were on average 57.56 ± 29.8 ms. Only when a positive bias was applied do NP detection events occur. When a negative bias is applied, the NPs are drawn to the electrode in the same compartment as the NPs; hence no translocation events take place. Examples of the spectra that were used to generate the time trace are shown in ESI. As shown in Figure 3 (red), the time trace of the 1364 $cm^{-1}$ vibrational band of MGITC was also generated. Further analysis using this vibrational band of MGITC reveals an average peak intensity of 3954 ± 1488 photons during the 88 seconds of positive 750 mV bias. As would be expected both time traces cross-correlate perfectly with each other as shown in figure 3b which shows the autocorrelation of the 1174 and 1364 $cm^{-1}$ vibrational bands along with the cross-correlation. It should be noted that the difference in signal to noise ratio between these time traces is the likely cause of the different amplitudes in the signal. A control cross-correlation was performed between the 1174 $cm^{-1}$ vibrational band and noise at 2327 $cm^{-1}$ which shows no correlation. This is

highly advantageous from a nanopore sensing perspective where different vibrational bands can either be used to distinguish between different analytes or alternatively can be used to increase the signal to noise.

Interestingly, during some translocation events, lower intensity vibrational bands of MGITC are also easily observed which is untrue for a bulk measurement. In some instances, the intensity of the 442 or 801 $cm^{-1}$ vibrational bands are even more intense than the typically stronger 1174 and 1364 $cm^{-1}$ vibrational bands. Figure 4a shows an example time trace of the 1174 $cm^{-1}$ vibrational band (blue) and the 442 $cm^{-1}$ vibrational band (red). As can be seen from the figure, occasionally the 442 $cm^{-1}$ vibrational band is more intense than the 1174 $cm^{-1}$ vibrational band of MGITC. This is highlighted in Figure 4b where example spectra representing intensity ratios, $R= I_{442\ cm^{-1}} / I_{1174\ cm^{-1}} = 0.11$, 1.87, and 2.88 are shown. Further examples are shown in the ESI Figure 11. The spectra show strong fluctuations in the vibrational band intensities which provides strong evidence that the NP are located within the nanopore boundaries since the wavelength of the maximum electric field enhancement is dependent on the position of the NP within the nanopore (Figure 1e, ESI Figure 7). As shown in Figure 4c, NPs freely diffusing in solution have an $R = 0.65 \pm 0.20$. This is increased to $0.70 \pm 0.45$ for NPs detected during translocations. The increase in the average ratio and the larger spread is likely due to the wavelength dependent enhancement factor obtained for different NP trajectories through the nanopore. R-values greater than 5 were also recorded and are shown in the ESI Figure 11. Although the 442 $cm^{-1}$ is typically weaker, a strong cross-correlation between the 442 $cm^{-1}$ and 1174 $cm^{-1}$ bands, due to the enhancement in signal obtained within a nanopore, is observed (see ESI Figure 12). In bulk, often this signal would be heavily suppressed due to the signal to noise ratio being lower. Importantly, regardless of the fluctuations created by the wavelength dependent enhancement, in all cases the spectral signature was sufficient to determine that the detected analyte was MGITC (see ESI Figure 13). This is very important, as the unique spectral signature extracted using SER(R)S-based detection can be used for analyte identification which previous nanopore detection methods have lacked.

Changing the applied bias directly affects the translocation frequency[9] as a result of a larger electric field generated at the nanopore. This was investigated using our nanopore system by changing the applied bias between 0 mV to 750 mV as shown in Figure 5. When no bias was applied (black), few translocation events were seen and were probably a result of diffusion through the probe volume. When a bias of 500 mV was applied (green), translocation events occurred with an average translocation time of $97.75 \pm 51.28$ ms (ESI Figure 9). Average signal intensity over a 30 second acquisition was $3486 \pm 1400$ photons. Increasing the applied bias to 750 mV (navy) increased the number of translocation events during a 30 second acquisition with an average signal intensity of $3884 \pm 1394$ photons. The average

translocation time decreased to 57.56 ± 29.8 ms (ESI Figure 9) when using a higher bias. In all cases, the bias also reversed to confirm that events are indeed due to translocation events (ESI Figure 14). A more efficient means of increasing the number of translocation events is to use arrays of nanopores along with simultaneous detection[9]. Although outside the scope of this manuscript, this is something we intend to pursue in the future.

An important requirement for a single analyte sensor is maintaining single analyte occupancy in the detection volume. The majority of single analyte techniques require low analyte concentrations or minimization of the probe volume dimensions to achieve this goal. For example, according to Poissonian statistics, the probability of having a single analyte in the 0.53 attoL detection volume defined by the nanopore is 0.003 for a 10 nM sample and 3.03e-7 for a 1 pM sample[41] . In this work the NP concentration used was 2.5 pM. This concentration was a compromise between maintaining a reasonable translocation frequency whilst avoiding a higher SERRS background signal from NPs dispersed in the bulk. Lower or higher NP concentrations are indeed possible with this kind of nanopore sensor. Lower NP concentrations will result in a reduced amount of translocation events, requiring longer overall experiment times. Increased concentrations will increase NP translocation frequency, however also increase the likelihood of having more than a single NP in the probe volume. For the 2.5 pM NP concentration, the likelihood of having two particles in the probe volume reduces to 4.5e-14. An important next step in the development of this sensor would be to allow the NPs to be loaded into the liquid compartment at the opposite side to the probe volume. This would remove the necessity to make the NPs appear invisible in the bulk (ie higher NP concentrations) which would increase translocation frequency. Primarily, NPs were loaded into the lower compartment as the gold possesses significantly less charge than the $SiN_x$ surface reducing electroosmotic drag on the NPs which increases the likelihood of translocations. A pure gold nanopore[42] would effectively shield the charge on the underlying $SiN_x$ surface and still maintain the electromagnetic enhancement..

An important finding of this study is the additional SERRS enhancement that occurs when using a metallic NP within a metallic nanopore. The average SERRS intensity from the time traces shown in Figures 2-4 are significantly higher than a bulk diffusion limited experiment. However, it is worth highlighting the high standard deviations in the peak intensity. We believe this to be related to the path that the NP travels through the nanopore. As shown in Figure 1d and Figure 1e (and ESI Figure 7a, b), the field enhancement depends greatly on the distance between the NP and nanopore. A NP travelling directly through the center of the nanopore will experience little enhancement (red line, Figure 1d). On the other hand, nanoparticles travelling near the edge of the nanopore (blue line, Figure 1d) will

experience an extremely high electric field enhancement. SERRS intensities higher than 20000 photons were detected in some cases (example spectra from binned photons ESI Figure 15). The EF was estimated by comparing the 1174 $cm^{-1}$ vibrational band intensity from a translocation event to that of a single diffusing particle and was calculated to range between 5 - 17. It should be stressed that this EF was solely due to the increase in the e-field intensity from the nanopore on the NP, aka comparing a SERRS to a SERRS event. Traditionally, EF is calculated by comparing a SERS to a Raman measurement, however since both the NP and nanopore are individually creating an electric field enhancement, only a comparison between the two SERRS measurements could be performed. Indeed the EF seen experimentally is lower than simulation, however, considering the multitude of factors influencing both the simulation and experiments (i.e. location of NP within the nanopore, NP size, nanopore size), the experimentally derived EFs are realistic values. It should be noted that other phenomena could be contributing to the high standard deviation in peak intensity which may be more pronounced or not seen in bulk measurements as a result of isolating a single NP. For example, if a NP dimer (or other linear NP aggregate) were to enter the nanopore, the detected signal could be originating from a single or few molecules, causing spectral and spatial variations in the vibrational bands of MGITC. This could be true from a single NP as well, if for example the NP were to come into contact with the NP wall.

To achieve the experimental realization of detecting a translocating NP through a nanopore, a larger number of dyes were loaded onto each nanoparticle ( ≈ 589 MGITC molecules/NP). This was to ensure that the NPs were detectable both in the bulk solution and during a translocation, which allowed for direct comparison in the EF generated between both systems. This MGITC/NP ratio used does not reflect the true LOD of the system. The enhancement provided by the nanopore allows for reduced analyte concentrations to be used. A dilution series was performed using equal NP concentrations with different MGITC concentrations to get an understanding of the LOD (ESI Figure 16). The LOD was confirmed to be approximately one dye molecule/NP at a 100 ms acquisition time and EM gain of 1. When coupled with the extra enhancement generated by the nanopore, this dye molecule/NP ratio could be detected at the time resolutions required for detecting translocation events. Importantly, the experimental setup and acquisition parameters allowed for entire spectra to be recorded at a spectral resolution of 0.65 nm over a spectral window of 128.6 nm and time resolution of 880 μs. An improved spectral resolution could be achieved, such as 0.32 nm, which would reduce the time resolution to 920 μs. The important thing is the full vibrational spectrum of MGITC was recorded in each acquisition which therefore can be applied to any other analytes, whether proof-of-principle or "real."

Future work in coupling metallic nanopores with SERS-based detection should be focused on generating the electromagnetic enhancement independent of the position of the NP within the nanopore. For example, a nanopore can be created in a nanovoid structure[43]. In this arrangement, the enhancement is generated after the nanoparticle has translocated through the nanopore. Simulations and experimentation has shown a strong coupling exists between NPs and metallic nanovoids[44, 45]. This interaction will no longer be governed by the NPs position in relation to the nanopore allowing NP stabilization methods, such as silica encapsulation, to be used. Stabilized NPs protect the analyte and can be placed in higher salt concentrations which will increase NP translocation frequency and could allow for multiplexing detection methods with electrical detection. Other geometries could be fabricated on the exit of the nanopore as well, such as sharp metallic tips which would generate greater enhancements than just the circular nanopore rim[32]. Different NP geometries could also be used as the analyte carrier, such as nanostars or nanoshells with would produce greater EFs and provide better plasmonic tenability. Circular corrugations placed around the nanopore[46] can also be used to pump more light into the nanopore entrance, increasing the electromagnetic enhancement felt by the analyte. Finally, efforts should be made so that the NPs travel through the nanopore into the probe volume allowing higher NP concentrations to be used increasing the translocation frequency and guaranteeing all detection events are from NP translocations.

In conclusion, this manuscript for the first time has shown the ability to use rapid SERRS-based detection with solid state nanopores. Current techniques used to detect translocation events through a nanopore lack the ability to extract vibrational information. In this study, the metallic membrane creates an electromagnetic interaction between the metallic NP and metallic nanopore which increases the SERRS intensity by a minimum of 5-17 times compared to NPs freely diffusing in solution. Such an enhancement allows for short acquisition times to be used and importantly lower analyte concentrations. Modeling confirmed that the electromagnetic enhancement was related to the distance between the NP and metallic nanopore wall. From the full spectra acquisitions, not only is analyte identification possible due to the analytes' unique vibrational spectrum, but multiple vibrational bands of the analyte can be investigated simultaneously. Fine tuning of parameters such as excitation wavelength and changing the size of the nanopore to match the nanopore size can produce greater signal enhancements. In addition, the enhancement can be tuned to enhance wavelengths that match the vibrational band(s) of interest.

Supporting Information

Schematic showing a typical ionic current blockade experiment using nanoparticles as an example, schematic describing the device fabrication, NP synthesis and characterization (SEM and DLS data of

NPs), UV-Vis of MGITC, schematic of different detection arrangements, simulated electric field enhancement as a function of NP location within nanopore, normalized maximum electric field enhancement vs. the vibrational spectrum of MGITC, histograms of NP translocation times, CV curve showing NP adsorption to a gold electrode, histograms and MGITC spectra representing the wavelength dependant enhancement, auto and cross-correlation analysis, MGITC spectra comparisons between bulk measurements and translocations, time traces of translocations at different applied biases, spectra of MGITC showing a very large EM enhancement, and dye/NP loading characterization. This material is available free of charge via the Internet at http://pubs.acs.org.

**Acknowledgments**

JBE has been funded in part by an ERC starting investigator grant and a Leverhulme Trust grant. SAM acknowledges the Leverhulme Trust and EPSRC for financial support and JC acknowledges the National Research Foundation of Korea (grant number R11-2008-0061852).

**References**


1. Fologea, D.; Gershow, M.; Ledden, B.; McNabb, D. S.; Golovchenko, J. A.; Li, J. *Nano Lett.* **2005**, *5*, 1905-1909.

2. Venkatesan, B. M.; Shah, A. B.; Zuo, J.-M.; Bashir, R. *Adv. Funct. Mater.* **2010**, *20*, 1266-1275.

3. Fologea, D.; Ledden, B.; McNabb, D. S.; Li, J. *Appl. Phys. Lett.* **2007**, *91*, 053901.

4. Meller, A.; Branton, D. *Electrophoresis* **2002**, *23*, 2583-2591.

5. Miles, B. N.; Ivanov, A. P.; Wilson, K. A.; Dogan, F.; Japrung, D.; Edel, J. B. *Chem. Soc. Rev.* **2013**, *42*, 15-28.

6. Storm, A. J.; Chen, J. H.; Ling, X. S.; Zandbergen, H. W.; Dekker, C. *Nat. Mater.* **2003**, *2*, 537-540.

7. Gierak, J.; Madouri, A.; Biance, A. L.; Bourhis, E.; Patriarche, G.; Ulysse, C.; Lucot, D.; Lafosse, X.; Auvray, L.; Bruchhaus, L.; Jede, R. *Microelectron. Eng.* **2007**, *84*, 779-783.

8. Fischbein, M. D.; Drndic, M. *Appl. Phys. Lett.* **2008**, *93*, 113107.

9. Chansin, G. A. T.; Mulero, R.; Hong, J.; Kim, M. J.; deMello, A. J.; Edel, J. B. *Nano Letters* **2007**, *7*, 2901-2906.

10. Chansin, G. A. T.; Hong, J.; Dusting, J.; deMello, A. J.; Albrecht, T.; Edel, J. B. *Small* **2011**, *7*, 2736-2741.

11. Hong, J.; Lee, Y.; Chansin, G. A. T.; Edel, J. B.; deMello, A. J. *Nanotechnology* **2008**, *19*, 165205.

12. Rutkowska, A.; Edel, J. B.; Albrecht, T. *ACS Nano* **2012**, *7*, 547-555.

13. Ayub, M.; Ivanov, A.; Hong, J.; Kuhn, P.; Instuli, E.; Edel, J., B.; Albrecht, T. *J. Phys.: Condens. Matter* **2010**, *22*, 454128.

14. Chang, H.; Kosari, F.; Andreadakis, G.; Alam, M. A.; Vasmatzis, G.; Bashir, R. *Nano Lett.* **2004**, *4*, 1551-1556.

15. Han, A.; Schurmann, G.; Mondin, G.; Bitterli, R. A.; Hegelbach, N. G.; de Rooij, N. F.; Staufer, U. *Appl. Phys. Lett.* **2006**, *88*, 093901-093903.

16. McNally, B.; Singer, A.; Yu, Z.; Sun, Y.; Weng, Z.; Meller, A. *Nano Lett.* **2010**, *10*, 2237-2244.

17. Soni, G. V.; Singer, A.; Yu, Z.; Sun, Y.; McNally, B.; Meller, A. *Rev. Sci. Instrum.* **2010**, *81*, 014301-014307.

18. Liu, H.; Zhang, L.; Lang, X.; Yamaguchi, Y.; Iwasaki, H.; Inouye, Y.; Xue, Q.; Chen, M. *Scientific Reports* **2011**, *1*,

19. Kneipp, K.; Wang, Y.; Kneipp, H.; Perelman, L. T.; Itzkan, I.; Dasari, R. R.; Feld, M. S. *Phys. Rev. Lett.* **1997**, *78*, 1667-1670.

20. Doering, W. E.; Nie, S. *J. Phys. Chem. B* **2001**, *106*, 311-317.

21. Wei, H.; Håkanson, U.; Yang, Z.; Höök, F.; Xu, H. *Small* **2008**, *4*, 1296-1300.

22. Cecchini, M. P.; Hong, J.; Lim, C.; Choo, J.; Albrecht, T.; deMello, A. J.; Edel, J. B. *Anal. Chem.* **2011**, *83*, 3076-3081.

23. Cecchini, M. P.; Turek, V. A.; Paget, J.; Kornyshev, A. A.; Edel, J. B. *Nat. Mater.* **2013**, *12*, 165-171.

24. Maher, R. C.; Maier, S. A.; Cohen, L. F.; Koh, L.; Laromaine, A.; Dick, J. A. G.; Stevens, M. M. *J. Phys. Chem. C* **2009**, *114*, 7231-7235.

25. Maher, R. C.; Dalley, M.; Ru, E. C. L.; Cohen, L. F.; Etchegoin, P. G.; Hartigan, H.; Brown, R. J. C.; Milton, M. J. T. *J. Chem. Phys.* **2004**, *121*, 8901-8910.

26. Cecchini, M. P.; Stapountzi, M. A.; McComb, D. W.; Albrecht, T.; Edel, J. B. *Anal. Chem.* **2011**, *83*, 1418-1424.

27. Huang, J.; Kim, K. H.; Choi, N.; Chon, H.; Lee, S.; Choo, J. *Langmuir* **2011**, *27*, 10228-10233.

28. Doering, W. E.; Nie, S. *Anal. Chem.* **2003**, *75*, 6171-6176.

29. Anmiv, S. P.; Talukder Zaki, N. J.; Kevin, J. F.; Rafael, M.; Prashanta, D.; Min Jun, K. *J. Phys.: Condens. Matter* **2010**, *22*, 454107.

30. Astier, Y.; Datas, L.; Carney, R.; Stellacci, F.; Gentile, F.; DiFabrizio, E. *Small* **2011**, *7*, 455-459.

31. Lan, W.-J.; Holden, D. A.; Zhang, B.; White, H. S. *Anal. Chem.* **2011**, *83*, 3840-3847.

32. Ivanov, A. P.; Instuli, E.; McGilvery, C. M.; Baldwin, G.; McComb, D. W.; Albrecht, T.; Edel, J. B. *Nano Lett.* **2010**, *11*, 279-285.

33. Turkevich, J.; Stevenson, P. C.; Hillier, J. *Discuss. Faraday Soc.* **1951**, *11*, 55-75.

34. Frens, G. *Nature* **1973**, *241*,

35. Turek, V. A.; Cecchini, M. P.; Paget, J.; Kucernak, A. R.; Kornyshev, A. A.; Edel, J. B. *ACS Nano* **2012**, *6*, 7789-7799.

36. Qian, X.; Emory, S. R.; Nie, S. *J. Am. Chem. Soc.* **2012**, *134*, 2000-2003.

37. Albrecht, T.; Li, W.; Ulstrup, J.; Haehnel, W.; Hildebrandt, P. *ChemPhysChem* **2005**, *6*, 961-970.

38. Albrecht, T.; Li, W.-W.; Haehnel, W.; Hildebrandt, P.; Ulstrup, J. *Bioelectrochemistry* **2006**, *69*, 193-200.

39. Albrecht, T.; Mertens, S. F. L.; Ulstrup, J. *J. Am. Chem. Soc.* **2007**, *129*, 9162-9167.

40. Svoboda, K.; Block, S. M. *Opt. Lett.* **1994**, *19*, 930-932.

41. Hill, E. K.; Mello, A. J. d. *Analyst* **2000**, *125*, 1033-1036.

42. Li, Y.; Chen, C.; Kerman, S.; Neutens, P.; Lagae, L.; Groeseneken, G.; Stakenborg, T.; Van Dorpe, P. *Nano Letters* **2013**, *13*, 1724-1729.

43. Cole, R. M.; Baumberg, J. J.; Garcia de Abajo, F. J.; Mahajan, S.; Abdelsalam, M.; Bartlett, P. N. *Nano Lett.* **2007**, *7*, 2094-2100.

44. Huang, F. M.; Wilding, D.; Speed, J. D.; Russell, A. E.; Bartlett, P. N.; Baumberg, J. J. *Nano Lett.* **2011**, *11*, 1221-1226.

45. Speed, J. D.; Johnson, R. P.; Hugall, J. T.; Lal, N. N.; Bartlett, P. N.; Baumberg, J. J.; Russell, A. E. *Chemical Communications* **2011**, *47*, 6335-6337.

46. Aouani, H.; Mahboub, O.; Devaux, E.; Rigneault, H.; Ebbesen, T. W.; Wenger, J. *Opt. Express* **2011**, *19*, 13056-13062.

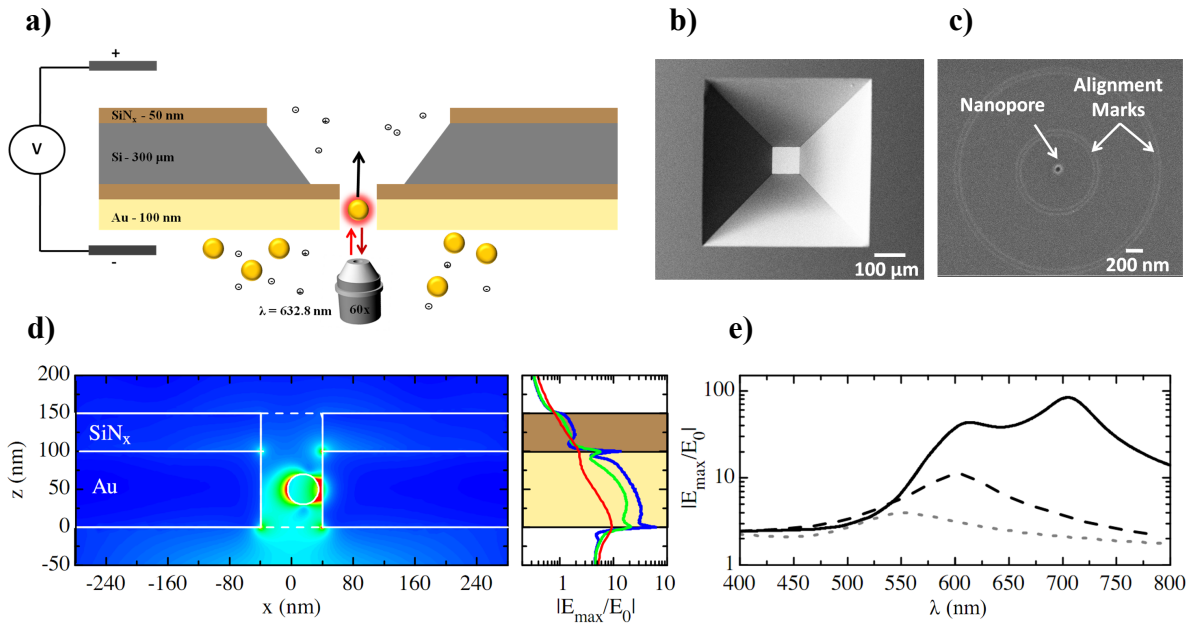


**Figure 1.** Schematic of optical NP detection with device images and simulated electric field enhancement. (a) Schematic of experimental arrangement. Nanoparticles were loaded into the lower compartment to avoid the negatively charged $SiN_x$ surface repelling the negatively charged nanoparticles from the nanopore. A positive bias was applied to drive the nanoparticle through the nanopore. (b) SEM image of microfabricated window and membrane. (c) SEM image of an 80 nm nanopore with two circular alignment marks around the pore. (d) Map of the electric field enhancement at 600 nm for a 40 nm diameter gold nanoparticle located in an 80 nm diameter nanopore filled with water, consisting of a 100 nm gold layer below a 50 nm $SiN_x$ layer, illuminated from the negative z direction. The saturated color scale ranges from 0 (blue) to 7 (red). The peak field enhancements generated at 600 nm by 40 nm diameter gold nanoparticles moving along vertical tracks through x=0 nm (red line), x=15 nm (green line) and x=17 nm (blue line) are traced. (e) Spectra of the maximum electric field enhancements generated by a 40 nm diameter gold nanoparticle located in water far away from the pore (dotted line), in the center of the nanopore at x, z=0 nm,0 nm (dashed line) and close to the nanopore wall at x, z=17 nm, 0 nm (solid line). The dipolar localized surface plasmon resonance of the sphere red shifts as the sphere enters the pore, splitting into a dipolar and a quadrupolar mode as the nanoparticle-wall distance is decreased.

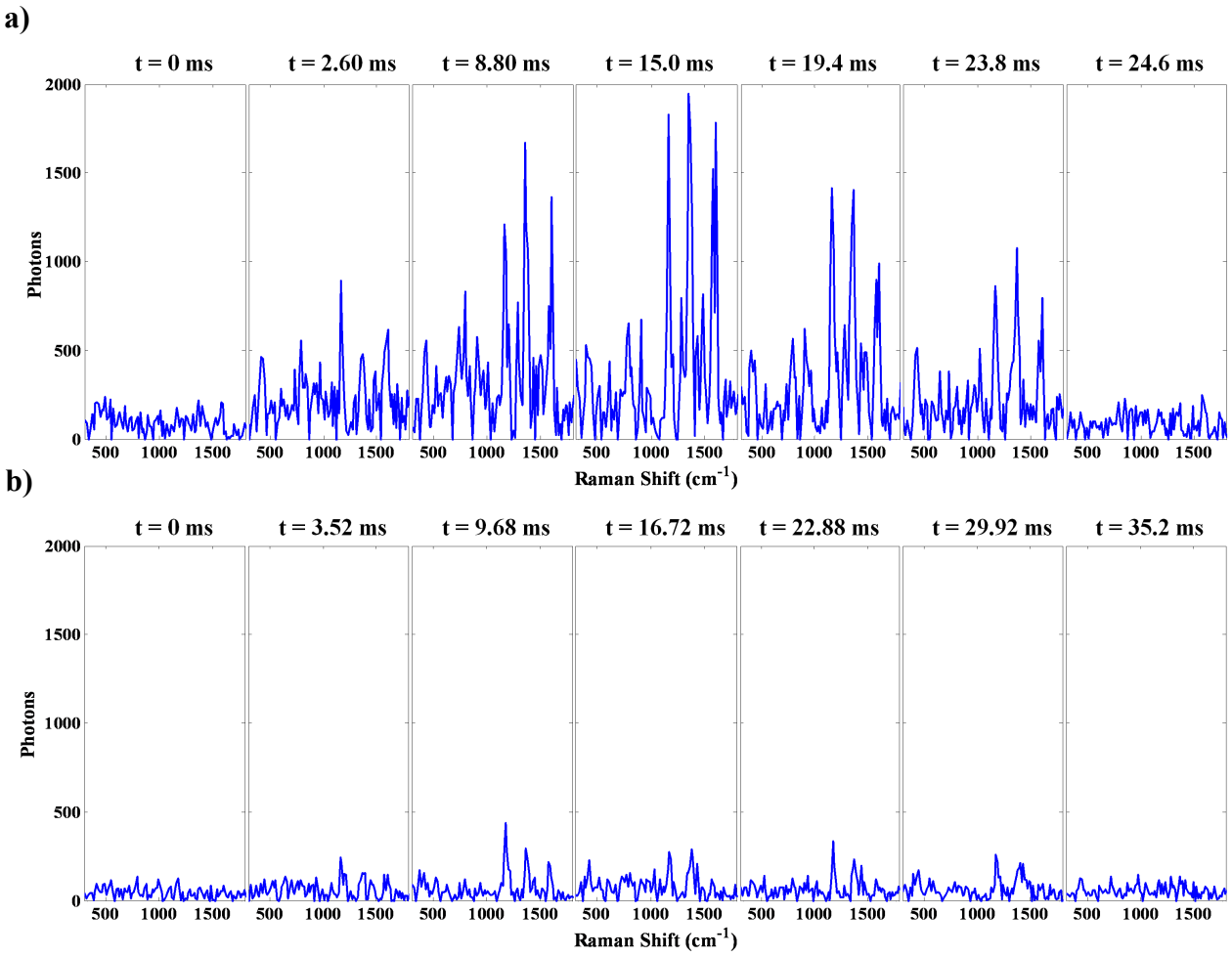


**Figure 2.** Spectra showing NP translocation and NP diffusion event. (a) An example of a 24.6 ms translocation using a 750 mV potential taken at a 880 μs acquisition time. This example shows the spectra acquired over the course of 24.6 ms representing a single NP translocating through the nanopore. (b) An example of a NP diffusing through the probe volume away from the nanopore. In this example a diffusion time of almost 30 ms is observed. Comparing the signal intensities between the nanoparticle translocation and diffusion event shows the signal enhancement generated between the nanoparticle and nanopore. A 320% signal increase of the 1174 $cm^{-1}$ vibrational band of MGITC is seen comparing the two detection events.

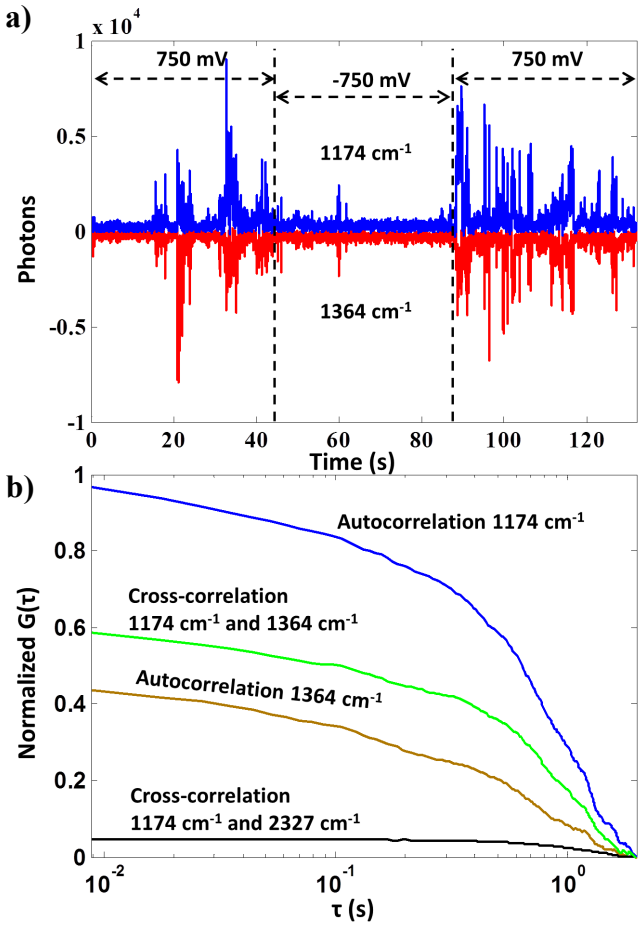


**Figure 3.** (a). Time trace comparing the 1174 (blue) and 1364 $cm^{-1}$ (red) vibrational bands of MGITC for a 132 second acquisition at an applied potential of 750 mV and -750 mV respectively. Translocations were only observed when a positive bias was applied. The time traces were recorded using an acquisition time of 880 µs and binned into groups of 8.8 ms. (b). A cross-correlation between the 1174 and 1364 $cm^{-1}$ vibrational band over the entire 132 second time trace reveal a near perfect correlation. Such an analysis highlights the strengths of using Raman-based detection coupled with nanopores. Unlike established nanopore detection techniques, where only a single signal is recorded, Raman spectroscopy can monitor multiple vibrational bands simultaneously. This has the possibility of increasing the accuracy of analyte detection, as noise from contaminants can also be identified.

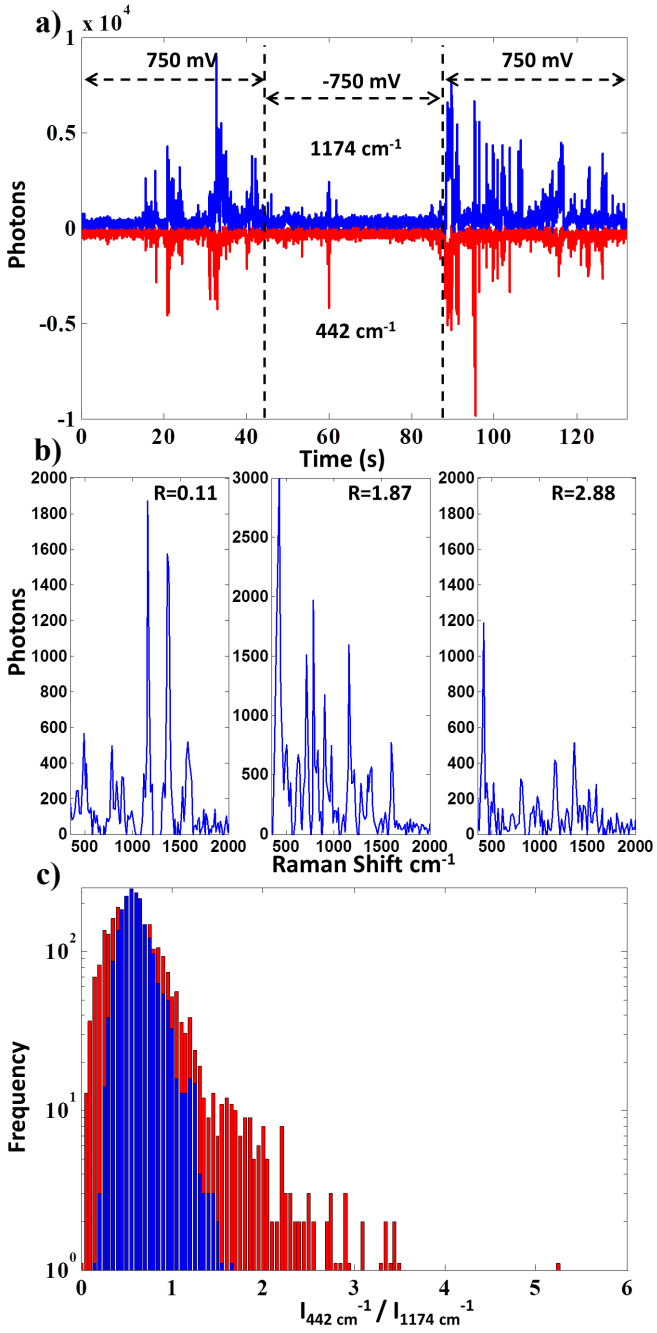


**Figure 4.** (a). Time trace comparing the 1174 (blue) and 442 $cm^{-1}$ (red) vibrational bands for the same acquisitions as shown in Figure 3. The wavelength dependence of the electric field enhancement created by the coupling of the metallic nanopore and NP selectively enhances different vibrational bands of MGITC as shown in (b). (b). Examples are shown for ratios ($R= I_{442\ cm^{-1}} / I_{1174\ cm^{-1}}$) (b) 0.11 (90.98 s) (c) 1.87 (95.38 s) (d) 2.88 (91.29 s). (c). Histograms of R for NPs labeled with MGITC for translocation events (red) and freely diffusing in solution (blue). The average ratio increases from 0.65 ± 0.20 to 0.70 ± 0.45 due to the interaction with the NP with the nanopore which enhances different vibrational bands

based on their wavelength.

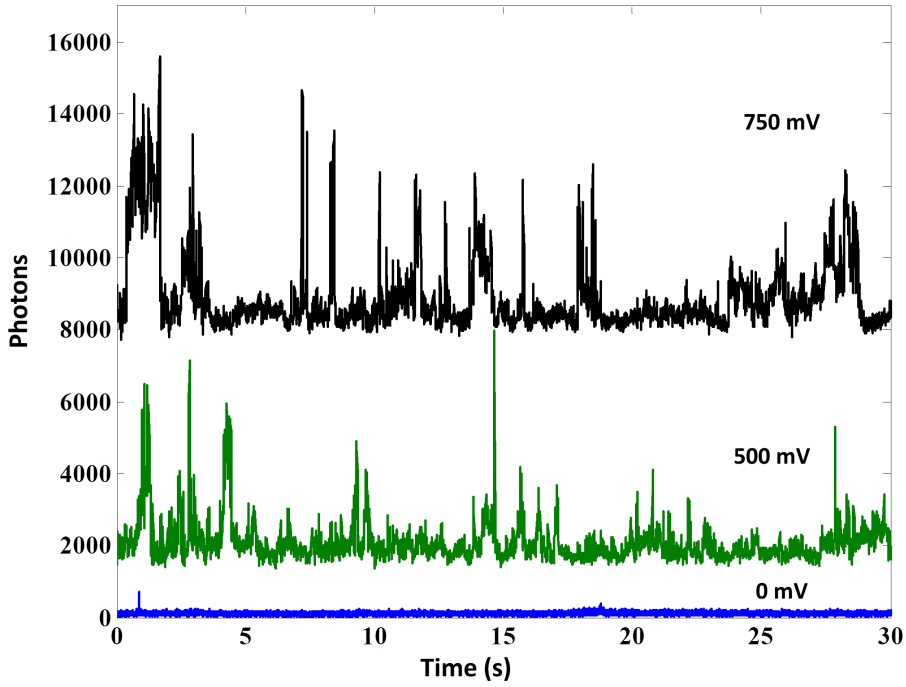


**Figure 5.** The effect of applied bias on the nanoparticle translocations frequency using the 1174 $cm^{-1}$ vibrational band. Again the detection events were recorded using an acquisition time of 880 µs and binned into groups of 8.8 ms. When no bias is applied (blue) no translocation events occur. When a positive bias is applied translocation events begin to occur (green/black). An increase in translocation events is seen when the bias is increased from 500 mV to 750 mV, a result of increasing the electric field responsible for driving the NPs through the nanopore.

TOC